Jurnal Kejuruteraan 38(3) 2026: 1499-1510
https://doi.org/10.17576/jkukm-2026-38(3)-39

Powder Characterization of Shape Memory Alloy (SMA) Nickel-Titanium (NiTi) and Numerical Simulation of Selective Laser Melting (SLM) Processing Parameters

Farhana Mohd Foudzi[a,b*], Intan Liyana Ramli[a,b], Nur Affiqah Dania Sazali[a], Wei Yin[a,b], Abu Bakar Sulong[a,b], Nabilah Afiqah Mohd Radzuan[a,b], Zainudin Sajuri[a,b] & Mohannad Salleh Hammadi Al-Furjan[c]

[a]*Advanced Manufacturing Research Group, Universiti Kebangsaan Malaysia, 43600 Bangi, Selangor, Malaysia*

[b]*Department of Mechanical and Manufacturing Engineering, Faculty of Engineering and Built Environment, Universiti Kebangsaan Malaysia, 43600 Bangi, Selangor, Malaysia*

[c]*College of Aerospace Engineering, Nanjing University of Aeronautics and Astronautics, 29 Yudao St. Nanjing, Jiangsu Province, China*

[*]*Corresponding author: farhana.foudzi@ukm.edu.my*

Received 8 August 2025, Received in revised form 8 December 2025
Accepted 8 January 2026, Available online 30 May 2026

ABSTRACT

This study was conducted to evaluate the suitability of Nickel-Titanium (NiTi) alloy powder, a type of Shape Memory Alloy (SMA), for 4D fabrication using Selective Laser Melting (SLM) technology. NiTi exhibits remarkable properties such as superelasticity and the shape memory effect, allowing it to return to its original shape. These characteristics make it highly valuable in biomedical applications such as orthopaedic implants and vascular stents, as well as in aerospace systems. However, conventional manufacturing methods often face significant limitations when processing NiTi due to its complex thermomechanical behavior, including high thermal sensitivity, rapid work hardening, and low thermal conductivity. The study involved physical characterization of NiTi powder using Particle Size Analysis (PSA), Field Emission Scanning Electron Microscopy (FESEM), Energy Dispersive X-ray Spectroscopy (EDX), and X-ray Diffraction (XRD) to determine particle morphology, size, and element composition. Additionally, Differential Scanning Calorimetry (DSC) was used to analyze phase transformation behavior between the martensite and austenite phases. The powder characterization was performed to analyze the feedstock and verify its suitability for SLM processing before fabrication, while the numerical simulation was conducted to identify the optimal linear energy density for future experimental work. Numerical simulation was conducted via Flow-3D AM software to study the influence of various linear energy densities (P/V ratios) on melt pool stability. Results indicated that a P/V ratio of 0.2 J/mm produced the most stable melt pool profile, offering the optimal balance between melting depth and thermal distribution. Overall, the findings demonstrate that NiTi powder is suitable for SLM applications, and numerical simulation plays a vital role in optimizing processing parameters to achieve high-performance fabrication outcomes.

Keywords: Nickel-Titanium (NiTi); Shape Memory Alloy (SMA); Selective Laser Melting (SLM); numerical simulation; 4D printing

INTRODUCTION

The manufacturing industry is undergoing a significant transformation driven by rapid technological advancement and evolving production demands. There has never been a greater need for creative production techniques that can satisfy demanding time-to-market needs, material performance standards, and ever more complicated design specifications. Industries including tooling, biomedical engineering, aerospace, and automotive are pushing the boundaries of traditional manufacturing techniques, which are frequently limited by high tooling costs, energy consumption (Valls & Le Bourdiec 2024) long lead times, material waste, and geometric restrictions (Valls & Le Bourdiec 2024). This continuing revolution has encouraged manufacturers and researchers to exploring more flexible and effective alternative fabrication technologies, particularly those that enable the rapid realization of

complex components without compromising mechanical performance or increasing production overhead (Bagherian & Kondala 2025; Becker & Grzesiak 2010; Charipar et al. 2014; Dalton et al. 2020; Khan et al. 2025; Korkmaz et al. 2022; S. Liu & Ding 2019; Ostendorf et al. 2017; Pessard et al. 2008; Roach et al. 2019; Tian et al. 2024). The growing demand for complex products, rapid production components, and the integration of smart functionalities into physical systems has intensified the pressure to innovate, driving the need for advanced manufacturing technologies that surpass the limitations of conventional subtractive methods (Becker & Grzesiak, 2010; Khan et al. 2025; Pessard et al. 2008). One of the most promising approaches to overcoming these manufacturing challenges is Additive Manufacturing (AM), commonly known as 3D printing. Unlike conventional subtractive techniques such as casting, forging, or machining, which remove material from a solid block, AM constructs components layer by layer, straight from computer-aided design (CAD) models. Additive manufacturing enables the fabrication of parts with unprecedented freedom in geometry, including internal cavities, lattice structures, and customized external features, all of which would be highly complex, expensive, or even impossible to create using traditional techniques (Khoo et al. 2018). In addition, AM offers shorter production cycles (Bacciaglia et al. 2020), greater design flexibility (J. Liu et al. 2020), and less material waste (Javaid et al. 2021). It also allows on-demand manufacturing, which reduces the need for inventory storage and enables localized production strategies, aligning with the principles of sustainable and just-in-time manufacturing.

In metal additive manufacturing, Powder Bed Fusion (PBF) has drawn the most attention among the several AM technologies, particularly the Selective Laser Melting (SLM) process, which selectively melts and fuses metallic powder particles in a predetermined pattern using a high-energy laser beam. This approach enables the production of fully dense metal parts with superior mechanical properties, high geometric accuracy, and smooth surface finishes can be produced with this method (Daoud et al. 2024; Kempen et al. 2011; Kuai et al. 2022; Swiercz & Oniszczuk-Swiercz, 2024). Due to these advantages, SLM has become an ideal technique used in industries where precision and performance are crucial, such as tooling, medical implants, and aerospace (DebRoy et al. 2018). Furthermore, SLM can process a wide range of metal alloys, enhancing its versatility in high-value manufacturing applications.

Beyond producing solid components, SLM also allows the fabrication of lightweight and high-strength designs through advanced geometrical control. Complex lattice structures such as body-centered cubic (BCC), gyroid, and diamond architectures can be produced with tailored mechanical properties and excellent energy absorption capabilities (Briones-Montemayor et al. 2025; Maconachie et al. 2019). Moreover, SLM supports design optimization through topology optimization and customized unit-cell design, allowing maximum stiffness and load-bearing capacity in high-performance applications (Xiao et al. 2018; L. Zhang et al. 2020).

However, in order to achieve high-performance SLM printing parts, careful control over process parameters such as laser power, scanning speed, hatch spacing, and layer thickness is necessary. Melt pool behavior, microstructure evolution, and defect formation are significantly influenced by these parameters, which are also directly related to volumetric and linear energy density (P/V) (Lu et al. 2024). Their interaction not only dictates how efficiently the material is melted and solidified but also determines thermal gradients, cooling rates, and phase stability within the printed component. Inadequate parameter selection can lead to process instabilities such as keyhole formation (Su et al. 2024), balling (Feng et al. 2022), cracking (Karlsson et al. 2019), or even incomplete fusion (C. Zhang et al. 2023), all of which can degrade the mechanical properties of the printed part. Therefore, parameter optimization remains an essential concern in developing repeatable, high-quality SLM processes.

SLM has shown a growing interest in Shape Memory Alloys (SMA), particularly Nickel-Titanium (NiTi) alloys. NiTi is unique because of its superelasticity and shape memory effect (SME), which enable it to regain its original shape when heated or unloaded. These functional characteristics make it ideal for aircraft components that need to be flexible in harsh environments, as well as biomedical devices such as orthopedic implants and stents (Yasa & Kruth, 2011). NiTi's ability to undergo reversible phase transformations under mechanical or thermal stimulus is the basis of its use in applications that demand smart, adaptive behavior. Despite its potential, the hardness, quick work-hardening, and heat sensitivity of NiTi make it difficult to fabricate using traditional techniques like welding and machining, which frequently result in phase instability or poor surface quality (Habijan et al. 2013).

Before fabricating the part using the SLM process, powder characterization was conducted to evaluate the suitability of the NiTi powder. Comprehensive characterization is essential for ensuring consistent powder quality, as it directly influences process stability, melt pool behavior, and the mechanical properties of the final component. The assessment of powder characteristics enables the detection of defects or irregularities such as contamination, oxidation, or non-uniform particle size that could compromise print quality or induce process instability. In research and development, characterization

also plays a pivotal role in understanding the material's behavior during phase transformation and grain evolution under thermal exposure. By tailoring powder morphology, composition, and thermal properties, researchers can optimize process parameters for improved printability and performance. Overall, this preliminary characterization step ensures that the NiTi powder meets the requirements for reliable SLM processing and lays the foundation for reproducible, high-quality fabrication outcomes.

An efficient method for creating NiTi components is offered by SLM, but its effectiveness depends on precisely controlling the temperature parameters to avoid problems like nickel evaporation, porosity, or microcracking. These defects not only compromise mechanical strength but also impair the alloy's functional response, such as delayed transformation temperatures or loss of superelasticity. Considering these difficulties, numerical simulation tools like Flow-3D AM are used to predict and optimize thermal behavior during SLM processing. These methods significantly reduce trial-and-error in actual fabrication by simulating temperature distribution, melt pool dynamics, and solidification behavior based on different process parameters (Chernyshikhin et al. 2021). Simulation allows for insight into complex thermo-fluid interactions and supports data-driven decisions in selecting appropriate printing parameters, reducing material waste, and accelerating process validation.

In this study, laser power and scanning speed were not analyzed independently but were varied proportionally to establish three values of linear energy density (LED = P/V) conditions of 0.1 J/mm, 0.2 J/mm, and 0.3 J/mm. These combinations were implemented in the Flow-3D AM simulation to investigate the influence of overall energy input on melt-pool morphology, thermal distribution, and fluid flow behavior during the SLM process. The selected ranges of laser power (130–190 W) and scanning speed (600–1000 mm/s) were based on values commonly reported for NiTi alloys in previous studies, ensuring realistic simulation conditions.

Therefore, the objective of this study is (1) to analyze the physical properties of NiTi SMA powder for the Selective Laser Melting (SLM) process, (2) to analyze the thermal properties of NiTi powder using Differential Scanning Calorimetry (DSC) technique, (3) to determine suitable printing parameters based on numerical simulation. In this study, powder characterization was performed to analyzed the feedstock and verify its suitability for SLM processing before fabrication, while the numerical simulation was conducted to identify the optimal linear energy density for future experimental work. Through this research, it is expected that an optimized framework for SLM-based NiTi fabrication can be established, contributing to the broader adoption of SMAs in advanced engineering systems.

METHODOLOGY

This study used a dual strategy that combines numerical modelling and experimental powder characterisation to fully evaluate the processability and thermal behaviour of NiTi Shape Memory Alloy (SMA) powder for Selective Laser Melting (SLM). The primary stages of the methodology are (i) the physical and (ii) thermal characterisation of the NiTi powder and (iii) the use of Flow 3D-AM software to numerically simulate the melt pool development. Figure 1 shows the research flowchart of this paper.

POWDER CHARACTERIZATION

The first part of this study focuses on analyzing the physical properties of Nickel-Titanium (NiTi) Shape Memory Alloy (SMA) powder to evaluate its suitability for the Selective Laser Melting process. Several characterization techniques were employed to assess the morphology, particle size distribution, and elemental composition of the powder. The powder was supplied by ORS Technologies Sdn. Bhd. with the as-received composition of 55.8 wt % Nickel and 44.2 wt % Ti. The supplied data indicated a Hall flow rate of 19.8 s/50 g, which is within the range for metal powders used in SLM (Altug-Peduk et al. 2018). The Particle Size Analysis (PSA) was carried out using a Malvern Mastersizer 2000 to determine the particle size distribution range (D_{10}, $D_{50,}$ D_{90}) of the NiTi powder. The tests were done 3 times, and the distribution values were averaged to get the precision data. These results indicated a particle size distribution, which is essential for ensuring uniform powder spreading and consistent layer deposition during the SLM process. The optimal size distribution is critical to minimize porosity and achieve a high relative density in the final product (Yan et al. 2024).

Next, the morphological characteristics of the powder were observed using Field Emission Scanning Electron Microscopy (FESEM). The analysis was conducted using a SUPRA 55VP microscope. The spherical morphology is particularly favorable for SLM as it promotes excellent flowability and facilitates uniform powder layering, both critical for maintaining part density and surface quality during laser melting (Jiang et al. 2022). To confirm the elemental composition of the powder, Energy Dispersive X-ray Spectroscopy (EDX) analysis was performed. This compositional consistency is essential to ensure reliable phase transformation behavior and mechanical performance

after SLM processing. Phase analysis was conducted using X-ray Diffraction (XRD) to identify the crystallographic phases present in the NiTi powder. The analysis was performed on the powders with Cu-Kα radiation (wavelength = 1.5406 Å). The dominance of the phase is crucial because it indicate whether the powder is in a high-temperature, stable phase suitable for superelastic behavior at room temperature (Chen et al. 2019).

Lastly, the thermal transformation characteristics of the NiTi powder were evaluated using Differential Scanning Calorimetry (DSC), NETZSCH-DSC 214 Polyma. This technique allowed the detection of transformation temperatures, including martensite start (M_s), martensite finish (M_f), austenite start (A_s), and austenite finish (A_f). These temperatures indicate the reversible phase transitions between martensite and austenite, which are responsible for the shape memory effect and superelastic behavior. The measurements were carried out at a range of temperatures from -50 ^oC to 250 ^oC with a rate of 10 °K/min in nitrogen gas (N_2). The suitable temperature range to capture the full transformation cycle, ensuring that the material responds correctly under thermal stimuli relevant to its target applications (Yu et al. 2023).

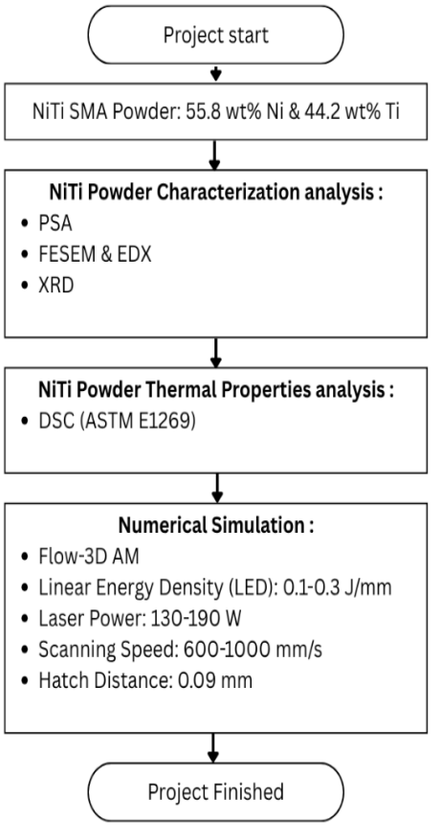

FIGURE 1. Research Flowchart

TABLE 1. Simulation parameter

Laser Power (W)	Scanning Velocity (mm/s)	LED (J/mm)
130	1000	0.1
160	800	0.2
190	600	0.3

NUMERICAL SIMULATION

The final part of this study focuses on numerical simulation to determine the optimal printing parameters for the SLM process. The simulation was conducted using Flow-3D AM, computational fluid dynamics (CFD) based software specialized for additive manufacturing. The primary focus was to investigate the effects of varying linear energy density (LED=P/V), on melt pool formation and thermal distribution during the fabrication of NiTi alloy using SLM through numerical simulation. At this step, laser power and scanning speed were adjusted to generate three LED conditions: 0.1 J/mm (low energy), 0.2 J/mm (medium energy), and 0.3 J/mm (high energy) while keeping hatch distance and layer thickness constant, with 0.09 mm and 0.03 mm, respectively. The laser power was varied between 150–200 W, and the scan speed ranged from 600–1000 mm/s to investigate the influence of energy input. The average particle size of the spherical NiTi powder was 38.29 μm, following a normal distribution between 3–53 μm. To ensure computational accuracy, the grid size was set to 3 μm in the melt pool region. This method was designed to estimate the effect of energy input on melt pool stability, temperature distribution, and fluid flow characteristics rather than to analyze the independent influence of each processing parameter.

Melt pool depth, temperature profiles, and heat-affected zones were analyzed to evaluate the stability of the process under different P/V values. This simulation approach provides predictive insights to guide the selection of suitable process parameters that would minimize defects such as porosity, lack of fusion, or keyhole formation, ultimately contributing to the fabrication of high-quality, functional NiTi components (Ninpetch et al. 2020). Table 1 shows the input parameters of the simulation. The laser absorptivity (A_o) was calculated using the following empirical formula in Equation 1, where ρ_o is DC resistivity of NiTi at 20°C, β_o is the temperature coefficient of resistance, λ is the laser wavelength, and T is the average melt pool temperature. All the input of the equation is summarizes in Table 2.

$$A_0=0.365(\rho_0[1+\beta_0(T-20)]/\lambda)^{0.5} \quad (1)$$

TABLE 2. Parameter in Laser Absorptivity

Parameter	Value
ρ_0 (DC resistivity of NiTi at 20°C)	1.1×10^{-6} Ω·m
β_0 (temp. coefficient of resistance)	6.6×10^{-4} °C^{-1}
λ (laser wavelength, Yb fiber laser)	1.06×10^{-6} m
T (avg. melt pool temperature).	1600°C

The heat transfer process in the simulation was governed by the energy conservation Equation 2, where ρ is the material density, C_p is the specific heat capacity, k_o is the thermal conductivity, and C_p represents the internal heat source term generated by laser irradiation. To ensure realistic heat exchange

$$\frac{\partial(\rho T)}{\partial t} + \nabla(\rho \mu T) = \nabla(\frac{k_0}{C_p}\nabla T) + S_r \quad (2)$$

During the Selective Laser Melting process, convective ($h = 15\ W/(m^2 \cdot K)$) and radiative ($\varepsilon = 0.35$) heat losses were applied to the top surface, while all other boundaries were defined as adiabatic. These boundary conditions accurately represent the thermal environment of the SLM process and prevent artificial heat flux through the sides and bottom of the computational domain. The inclusion of these parameters enhances both the physical accuracy and reproducibility of the numerical model, allowing for more reliable prediction of melt pool behavior and temperature distribution.

RESULTS AND DISCUSSION

The physical characterization of NiTi powder was crucial in determining its suitability for the Selective Laser Melting (SLM) process. The Particle Size Analysis (PSA) results, illustrated in Figure 2, revealed that the NiTi powder exhibited a relatively narrow and uniform particle size distribution. The median particle size D_{50} value recorded was 38.29 µm, while D_{10} and D_{90} were 26.32 µm and 55.67 µm, respectively. These values indicate that 10 % of the particles are smaller than 26.32 µm, 50% are smaller than 38.29 µm, and 90% are smaller than 55.67 µm, defining a particle size distribution range of approximately 26–56 µm. Table 2 shows the summary of powder distribution together with the explanation. This distribution falls within the recommended range for metal additive manufacturing powders to ensure good flowability and high packing density. According to Yan et al. (2024),maintaining a well-balanced distribution avoids problems like incomplete melting or powder agglomeration, which could otherwise lead to surface defects or weak bonding between layers. Powders with a smaller particle size generally exhibit better formability (Wang et al. 2012). In addition, larger particle sizes above 53 µm can lead to fewer but larger cavities (M. Wang et al. 2023). Nevertheless, powder with a particle size of less than 150 µm is suitable for use in additive manufacturing technology. In addition, the increase in particle size also increases the transformation temperature (Wang et al. 2022). To further quantify the width of the distribution, the Span was calculated using the relation $(D_{90}–D_{10})/D_{50}$, resulting in a value of 0.77. The narrow distribution of particle size indicates that the powder is evenly distributed. A uniform particle size distribution is essential to minimize interlayer voids during the recoating step in SLM, which directly impacts the melt pool stability, mechanical integrity of the final part, and achieving high-density parts. Furthermore, it also reduces the probability of voids and defects in the final product (Sagar et al. 2020, 2022; Spierings et al. 2011). The optimized size range also supports efficient energy absorption and melting behavior, contributing to consistent thermal conductivity across layers and minimizing residual stresses.

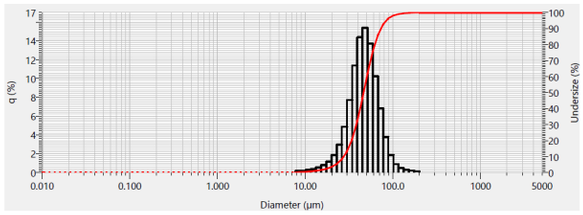

FIGURE 2. Particle Size Analysis (PSA)

TABLE 2. Powder distribution result from PSA

Symbol	Value (µm)	Description
D10	26.32 µm	10% of the particles are smaller than 26.32 µm.
D50	38.29 µm	50% of the particles are smaller than 38.29 µm. This value is also called the median diameter because it divides the distribution into two equal halves (smaller and larger particles).
D90	55.67 µm	90% of the particles are smaller than 55.67 µm.

As shown in Figure 3, Field Emission Scanning Electron Microscopy (FESEM) revealed that the NiTi powder particles were primarily spherical in shape and had smooth surface textures. During the layer deposition process, spherical morphology is crucial for improving powder flow, which is necessary to achieve uniform layer thickness and prevent powder bed defects. The smoothness and sphericity also promote better packing efficiency and reduce the risk of trapped voids. The occurrence of irregular

or angular particles was minimal, which is beneficial, as such particles tend to have poor flowability and may lead to agglomeration or inconsistent melting during laser scanning. This, in turn, could result in poor layer fusion, microcracks, or increased porosity (Jiang et al. 2022). Figure 4 presents the results of Energy Dispersive X-ray Spectroscopy (EDX) conducted to determine the elemental composition of the NiTi powder. The EDX analysis confirmed that the NiTi powder consisted of approximately 57.1 wt% Nickel (Ni), 38.5 wt% Titanium (Ti), 2.7 wt% Carbon (C), and 1.7wt% Oxygen (O).

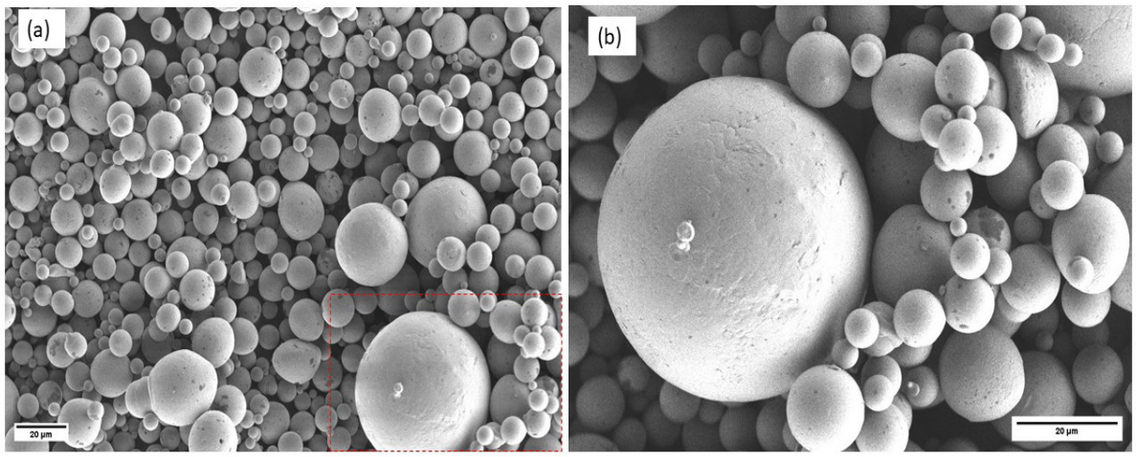

FIGURE 3. FESEM Microscopic at (a) 500 (b) 1000 magnification

The comparison of the powder values is summarised in Table 5. The EDX results indicate an increase in Ni content (~1.34%) and slightly higher levels of oxygen and carbon. These differences may be attributed to several aspects, including handling exposure during sample preparation and surface oxidation of the powder. The powder was supplied in a non-vacuum container, which may have exposed it to the environment and slightly altered its composition. This has also led to minor surface oxidation. Furthermore, the composition measurement method used in this study may differ from those used by the manufacturer. Despite that, the composition values reported by the manufacturer for Nickel and Titanium are consistent with those reported by previous researchers (Yang et al. 2019; Zhan et al. 2021). Maintaining a precise Ni/Ti ratio is critical because minor deviations can shift transformation temperatures, adversely affecting superelasticity and the shape memory effect (SME). In addition, trace amounts of carbon (2.7%) and oxygen (1.7%) were detected, likely resulting from surface oxidation during powder storage or handling. Although these levels are within acceptable thresholds, excessive oxygen or carbon could lead to the formation of undesired phases or brittle oxide layers during processing. These findings align with Garrido et al. (2024), who emphasized the importance of chemical consistency to preserve NiTi's functional performance throughout the SLM process. According to Speirs et. al 2016, oxygen content significantly influences the transformation temperatures of NiTi alloys (Speirs et al. 2016). Higher oxygen levels can lead to the formation of oxides such as Ti_4Ni_2O, which can embrittle the alloy and alter its transformation temperatures (Speirs et al. 2016; L. Wang et al. 2012; M. Wang et al. 2023). Meanwhile, carbon contamination is typically introduced during the melting process, which can stabilize unwanted phases such as TiC, which can affect the martensitic transformation temperatures and enthalpy changes (Otubo et al. 2006, 2008).

Subsequently, X-ray Diffraction (XRD) analysis presented in Figure 5 confirmed the presence of the B2 austenite phase, the primary phase responsible for superelastic behavior in NiTi alloys. The absence of significant martensitic or secondary phases suggests that the powder had not undergone any prior thermal cycling that could destabilize the desired crystallographic structure. The findings are consistent with the study by Yan et al. 2024, which also identified B2 austenite as the dominant phase. The presence of the B2 phase at room temperature confirms the material's readiness for SLM processing, especially since post-processing heat treatments could later be used to tune the final functional properties. Retention of this phase pre-processing is essential for ensuring that the transformation behavior will occur correctly upon heating and cooling, which is central to applications such as biomedical implants, sensors, and actuators.

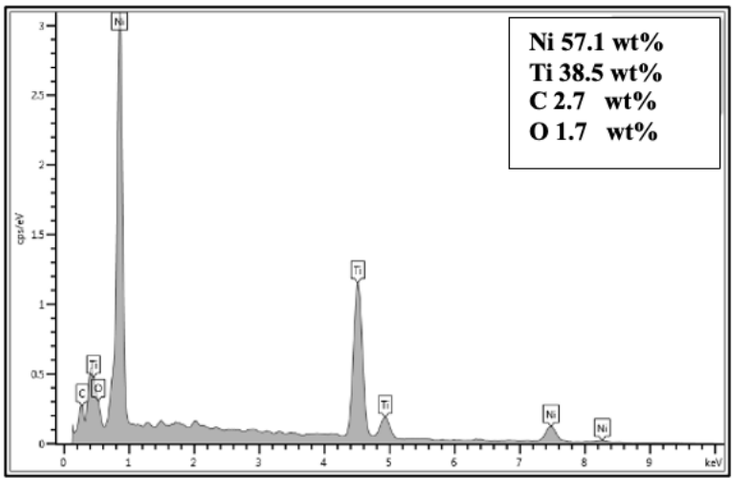

FIGURE 4. EDX Analysis

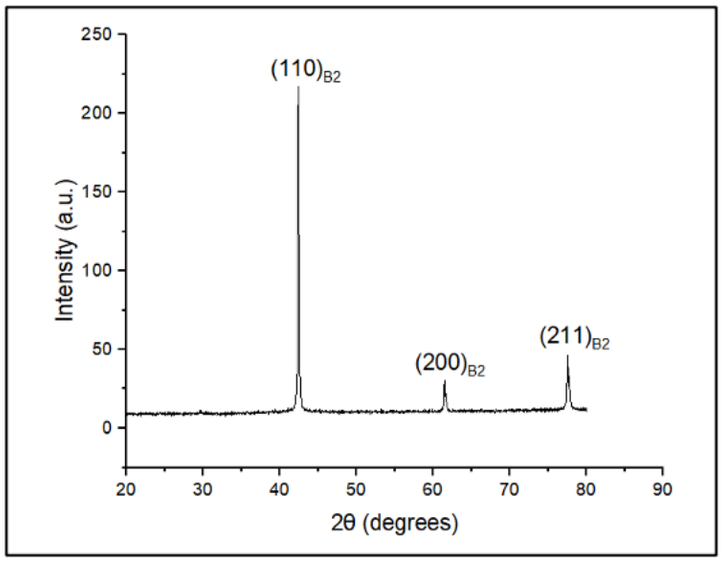

FIGURE 5. XRD Results

Differential Scanning Calorimetry (DSC) was employed to determine the thermal transformation characteristics of the NiTi powder. As shown in Figure 6, the Austenite Start (A_s) and Finish (A_f) temperatures were measured at -8.2°C and 35.24°C, respectively. Similarly, Martensite Start (M_s) and Finish (M_f) temperatures were identified at 23.15°C and -29.6°C. These transformation temperatures are typical of NiTi alloys intended for superelastic and SME applications.

The DSC curve exhibited a clear two-way transformation, with distinct endothermic and exothermic peaks associated with austenite and martensite phase changes. This behavior confirms that the NiTi powder retains its phase transformation characteristics, indicating suitability for temperature sensitive environments and functional applications. The suitability of these transformation temperatures also aligns with previous studies, where NiTi alloys with similar DSC profiles were reported to exhibit excellent functional performance in biomedical and actuator applications (Yan et al. 2024)

Moreover, the DSC data serves as a critical reference in the numerical modeling of SLM, where knowledge of transformation thresholds is necessary to predict post-processing phase composition and mechanical properties. Incorporating such data ensures that melt pool simulations reflect the actual thermal responses of the material, reducing the likelihood of phase instability post-fabrication.

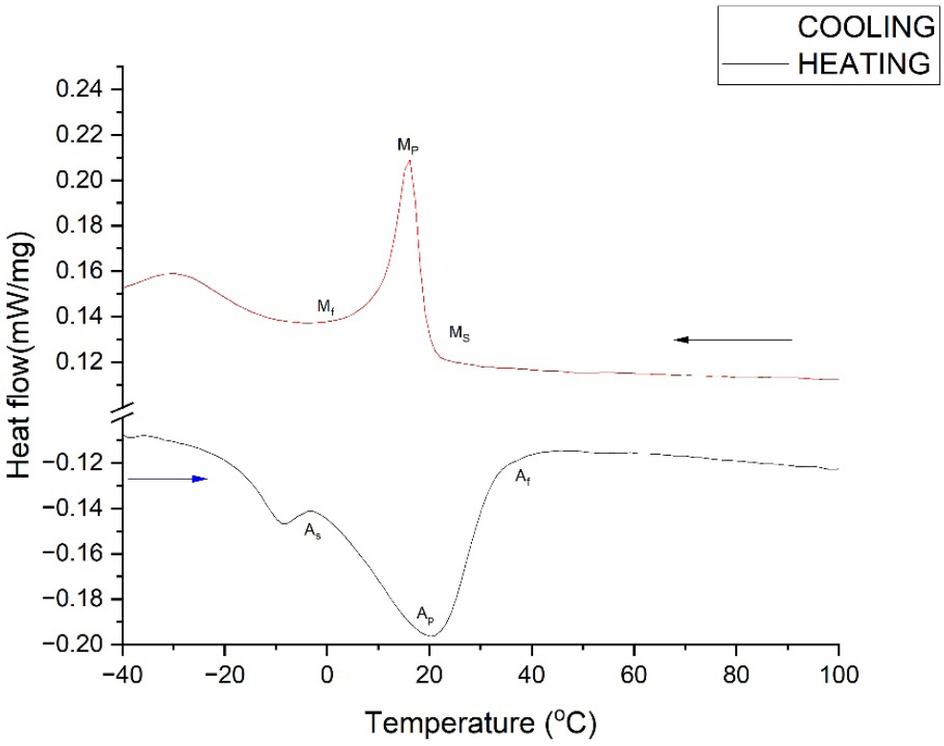

FIGURE 6. Heat Transformation of NiTi alloy powder

Numerical simulations were conducted using Flow-3D AM software to analyse melt pool formation under different linear energy density (P/V) conditions during the Selective Laser Melting (SLM) process. Three P/V ratios were evaluated using 0.1 J/mm (low energy), 0.2 J/mm (medium energy), and 0.3 J/mm (high energy). The simulations provided valuable insights into the thermal behavior, melt pool depth, and fluid flow dynamics during laser-material interaction. Figure 7(a)-(c) illustrates that the maximum temperature of the deposited layer reaches 1723K at direct laser irradiation. During selective laser melting (SLM), the melting and forming properties of NiTi alloys vary significantly with temperature. The lowest effective melting temperature is approximately 1350 K, corresponding to the solid-liquid eutectic point of the NiTi alloy (where $TiNi_3$ begins to melt). At this point, the material enters a fully liquefied state and possesses good fluidity. The optimal forming range is 1400–1650 K, where the molten pool exhibits moderate fluidity, facilitating uniform solidification and microstructure control. It also effectively suppresses Ni volatilization and reduces porosity, resulting in high density and excellent forming quality. When the temperature exceeds 1700 K, Ni readily volatilizes, leading to compositional segregation, molten pool instability, severe spattering, and a high risk of defects such as porosity and cracks. Therefore, this temperature range is considered a high-temperature risk zone. At the lowest energy input (0.1 J/mm) show in Figure 7(a), the simulation indicated the formation of a shallow and narrow melt pool, with inadequate penetration and localized heating near the surface. This condition suggested a high risk of defects such as porosity and lack-of-fusion due to insufficient melting. In contrast, the medium energy setting (0.2 J/mm) in Figure 7(b) demonstrated an optimal balanced melt pool with stable depth and width, suitable for full layer fusion without causing excessive thermal stress. The simulation showed uniform temperature gradients and symmetrical fluid flow patterns, minimizing the risk of defects while ensuring good microstructural consistency. The fluid flow within the melt pool was smooth and symmetrical, minimizing risks of thermal stress accumulation and microstructural inhomogeneity. Good melt pool formation is critical in SLM because it directly influences the part's density, mechanical strength, surface quality, and microstructure consistency. Uniform and stable melt pools help avoid common defects such as pores, cracks, and elemental segregation, all of which can degrade the mechanical performance and longevity of NiTi components (Wang et al. 2022).

.

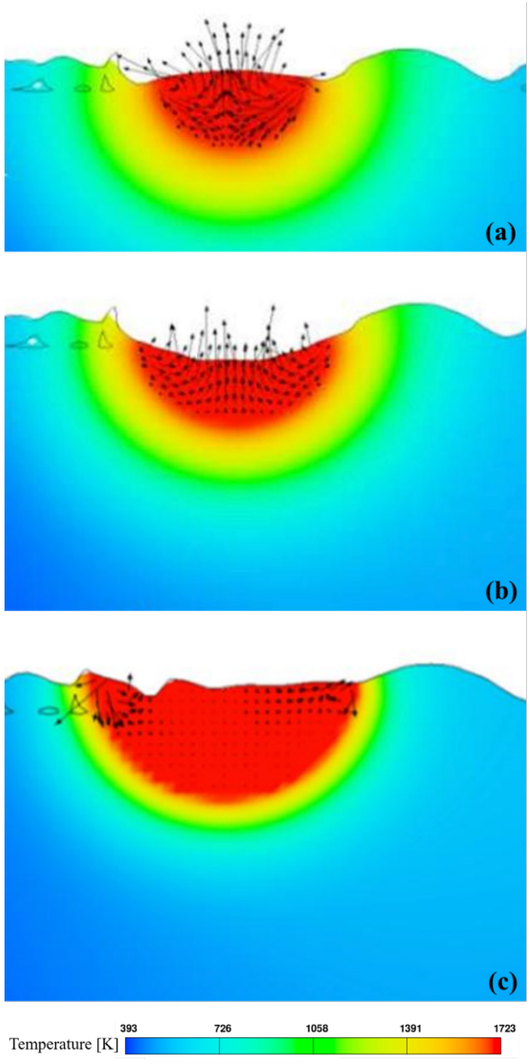

FIGURE 7. Simulations result for P/V (a) 0.1 J/mm (b) 0.2 J/mm (c) 0.3 J/mm

Figure 7(c) shows the highest energy input (0.3 J/mm), the simulation revealed excessive melt pool depth and width. It also shows a wide high-temperature zone, which maximizes the risk of defects. This condition raised concerns regarding nickel evaporation and microstructural instability due to overheating.

Overall, the simulation results identified the P/V ratio of 0.2 J/mm as the most favorable, providing a balanced energy input for stable melt pool formation and defect minimization. This phase of the study highlights the importance of numerical simulation in optimizing process parameters, reducing trial-and-error in experimental work, and ensuring high-quality fabrication of NiTi components via SLM.

CONCLUSION

In summary, this study conducted a comprehensive powder characterization of the NiTi alloy supplied by the manufacturer. The analyses included Particle Size Analysis (PSA), Field Emission Scanning Electron Microscopy (FESEM), Energy Dispersive X-ray Spectroscopy (EDX), and X-ray Diffraction (XRD) to evaluate the powder's suitability for Selective Laser Melting (SLM) applications. The NiTi powder exhibited a narrow particle size distribution with D_{10} = 26.32 µm, D_{50} = 38.29 µm, and D_{90} = 55.67 µm, corresponding to a Span of 0.77. This range is within the recommended values for SLM, supporting process stability, consistent melt pool behaviour, and optimal mechanical properties in the final component. The FESEM analysis revealed that the powder particles were mainly spherical and smooth, with only a few irregular or angular particles. Such morphology is beneficial because irregular particles tend to exhibit poor flowability, increasing the likelihood of agglomeration, incomplete melting, or porosity during layer deposition. Although slight variations were observed between the EDX composition values and those reported by the manufacturer, the manufacturer's composition remains consistent with findings from previous studies, confirming the reliability of the supplied powder. The XRD analysis confirmed the presence of the B2 austenite phase at room temperature, indicating that the powder is structurally suitable for SLM processing. The Differential Scanning Calorimetry (DSC) analysis revealed the thermal transformation characteristics of the NiTi alloy, where the Austenite Start (A□) and Austenite Finish (A_f) temperatures were measured at –8.2 °C and 35.24 °C, respectively, while the Martensite Start (M□) and Martensite Finish (M_f) temperatures were 23.15 °C and –29.6 °C. The numerical simulation using Flow-3D AM demonstrated that the linear energy density (P/V) ratio of 0.2 J/mm produced the most stable melt pool with balanced thermal distribution, indicating an optimal condition for SLM processing. These results highlight the value of numerical modelling in predicting suitable process parameters during the early stages of development. Overall, the powder characterization confirms the readiness of the NiTi feedstock for SLM processing, while the simulation results identify the optimal linear energy density for future experimental validation. The next phase of this research will involve experimental SLM fabrication using the same NiTi powder and the predicted processing parameters.

ACKNOWLEDGEMENT

The authors would like to acknowledge Center for Research and Instrumentation UKM (CRIM), Universiti Kebangsaan Malaysia for the financial support through Geran Universiti Penyelidikan (GUP-2024-084) for this study. Authors would also like to acknowledge ORS Technologies Sdn. Bhd. for providing the required facilities and knowledge transfer support to complete this study.

DECLARATION OF COMPETING INTEREST

None.

REFERENCES

Altug-Peduk, G. S., Dilibal, S., Harrysson, O., Ozbek, S. & West, H. 2018. Characterization of Ni–Ti alloy powders for use in additive manufacturing. *Russian Journal of Non-Ferrous Metals* 59(4): 433–439. doi:10.3103/S106782121804003X

Bacciaglia, A., Ceruti, A. & Liverani, A. 2020. Additive manufacturing challenges and future developments in the next ten years. In *Lecture Notes in Mechanical Engineering*, 891–902. doi:10.1007/978-3-030-31154-4_76

Bagherian, A. & Kondala, M. 2025. Smart factory technologies and their transformative implications: A Blavaan and Bayesian SEM. *Total Quality Management and Business Excellence* 36(5–6): 453–476. doi:10.1080/14783363.2025.2458257

Becker, R. & Grzesiak, A. 2010. Rapid manufacturing in automation applications. In *Innovative Developments in Design and Manufacturing: Advanced Research in Virtual and Rapid Prototyping*, 333–338.

Briones-Montemayor, M. J., Guzmán-Nogales, R., Majari, P., Estrada-Díaz, J. A., Elías-Zúñiga, A., Olvera-Trejo, D., Martínez-Romero, O. & Perales-Martínez, I. A. 2025. Enhanced mechanical performance of SLM-printed Inconel 718 lattice structures through heat treatments. *Metals* 15(7). doi:10.3390/met15070686

Charipar, N. A., Charipar, K. M., Kirleis, M. A., Kim, H., Auyeung, R. C. Y., Mathews, S. A. & Piqué, A. 2014. Hybrid manufacturing technologies for electromagnetic structures. In *International Conference on Digital Printing Technologies*, 129–132.

Chen, X., Liu, K., Guo, W., Gangil, N., Siddiquee, A. N. & Konovalov, S. 2019. The fabrication of NiTi shape memory alloy by selective laser melting: A review. *Rapid Prototyping Journal* 25(8): 1421–1432. doi:10.1108/RPJ-11-2018-0292

Chernyshikhin, S. V., Firsov, D. G. & Shishkovsky, I. V. 2021. Selective laser melting of pre-alloyed NiTi powder: Single-track study and FE modeling with heat source calibration. *Materials* 14(23). doi:10.3390/ma14237486

Dalton, P. D., Woodfield, T. B. F., Mironov, V. & Groll, J. 2020. Advances in hybrid fabrication toward hierarchical tissue constructs. *Advanced Science* 7(11). doi:10.1002/advs.201902953

Daoud, M. A., Hayani Mechkouri, M., Chairi, Y. & Reklaoui, K. 2024. Design of a benchmark part with recent design rules for selective laser melting. In *Springer Tracts in Additive Manufacturing*, 199–205. doi:10.1007/978-3-031-32927-2_18

DebRoy, T., Wei, H. L., Zuback, J. S., Mukherjee, T., Elmer, J. W., Milewski, J. O., Beese, A. M., Wilson-Heid, A., De, A. & Zhang, W. 2018. Additive manufacturing of metallic components—Process, structure and properties. *Progress in Materials Science* 92: 112–224. doi:10.1016/j.pmatsci.2017.10.001

Feng, E.-H., Wang, X.-Q., Han, X., Zhou, Z.-W., Kang, N., Wang, Q.-Z., Zhao, C.-L. & Lin, X. 2022. Process parameters optimization of Ti6Al4V fabricated by selective laser melting. *Powder Metallurgy Technology* 40(6): 555–563. doi:10.19591/j.cnki.cn11-1974/tf.2021040008

Garrido, C., Perosanz, S., Elliott, A., Simoes, M. & Barba, D. 2024. On the effect of the processing parameters in microstructure and thermomechanical properties of LPBF NiTi shape memory alloys. *Journal of Materials Research and Technology* 33: 2414–2429. doi:10.1016/j.jmrt.2024.09.155

Habijan, T., Haberland, C., Meier, H., Frenzel, J., Wittsiepe, J., Wuwer, C., Greulich, C., Schildhauer, T. A. & Köller, M. 2013. The biocompatibility of dense and porous nickel-titanium produced by selective laser melting. *Materials Science and Engineering C* 33(1): 419–426. doi:10.1016/j.msec.2012.09.008

Javaid, M., Haleem, A., Singh, R. P., Suman, R. & Rab, S. 2021. Role of additive manufacturing applications towards environmental sustainability. *Advanced Industrial and Engineering Polymer Research* 4(4): 312–322. doi:10.1016/j.aiepr.2021.07.005

Jiang, H., Xi, R., Li, X., Kustov, S., Van Humbeeck, J. & Wang, X. 2022. Structure, martensitic transformation, and damping properties of functionally graded NiTi shape memory alloys fabricated by laser powder bed fusion. *Materials* 15(14). doi:10.3390/ma15145073

Karlsson, D., Marshal, A., Johansson, F., Schuisky, M., Sahlberg, M., Schneider, J. M. & Jansson, U. 2019. Elemental segregation in an AlCoCrFeNi high-entropy alloy—A comparison between selective laser melting and induction melting. *Journal of Alloys and Compounds* 784: 195–203. doi:10.1016/j.jallcom.2018.12.267

Kempen, K., Yasa, E., Thijs, L., Kruth, J.-P. & Van Humbeeck, J. 2011. Microstructure and mechanical properties of selective laser melted 18Ni-300 steel. *Physics Procedia* 12: 255–263. doi:10.1016/j.phpro.2011.03.033

Khan, M. S., Hameed, S. & Dahri, A. S. 2025. Production sector dynamics: Technological advances in manufacturing and production. In *Converging Economic Policy, Corporate Strategy, and Technology for Emerging Economies*, 135–154. doi:10.4018/979-8-3693-5723-1.ch007

Khoo, Z. X., Liu, Y., An, J., Chua, C. K., Shen, Y. F. & Kuo, C. N. 2018. A review of selective laser melted NiTi shape memory alloy. *Materials* 11(4). doi:10.3390/ma11040519

Korkmaz, M. E., Waqar, S., Garcia-Collado, A., Gupta, M. K. & Krolczyk, G. M. 2022. A technical overview of metallic parts in hybrid additive manufacturing industry. *Journal of Materials Research and Technology* 18: 384–395. doi:10.1016/j.jmrt.2022.02.085

Kuai, Z., Li, Z., Liu, B., Liu, W. & Yang, S. 2022. Effects of remelting on the surface morphology, microstructure and mechanical properties of AlSi10Mg alloy fabricated by selective laser melting. *Materials Chemistry and Physics* 285. doi:10.1016/j.matchemphys.2022.125901

Liu, J., Liu, S., Yang, X., Li, A., Shi, M., Zhang, G., Zhang, Z. & Han, S. 2020. Progress in lightweight application research of additive manufacturing technology. *Materials China* 39(2): 163–168. doi:10.7502/j.issn.1674-3962.201808002

Liu, S. & Ding, Y. 2019. Wire-based direct metal deposition with Ti6Al4V. *Proceedings of SPIE: The International Society for Optical Engineering* 10909. doi:10.1117/12.2510521

Lu, H. Z., Zhou, Z. J., Yang, Y., Wang, R. C., Ma, H. W., Cai, W. S., Zhu, D. Z. & Yang, C. 2024. Effect of heat treatment on the microstructure and superelasticity of NiTi alloy via selective laser melting. *Journal of Materials Research and Technology* 30: 1044–1055. doi:10.1016/j.jmrt.2024.03.148

Maconachie, T., Leary, M., Lozanovski, B., Zhang, X., Qian, M., Faruque, O. & Brandt, M. 2019. SLM lattice structures: Properties, performance, applications and challenges. *Materials and Design* 183. doi:10.1016/j.matdes.2019.108137

Ninpetch, P., Kowitwarangkul, P., Mahathanabodee, S., Chalermkarnnon, P. & Ratanadecho, P. 2020. A review of computer simulations of metal 3D printing. *AIP Conference Proceedings* 2279. doi:10.1063/5.0022974

Ostendorf, A., Neumeister, A., Dudziak, S., Passinger, S. & Stampfl, J. 2017. Micro- and nano-parts generated by laser-based solid freeform fabrication. In *Advances in Laser Materials Processing: Technology, Research and Applications*, 595–633. doi:10.1016/B978-0-08-101252-9.00020-0

Otubo, J., Rigo, O. D., Coelho, A. A., Neto, C. M. & Mei, P. R. 2008. The influence of carbon and oxygen content on the martensitic transformation temperatures and enthalpies of NiTi shape memory alloy. *Materials Science and Engineering A* 481–482: 639–642. doi:10.1016/j.msea.2007.02.137

Otubo, J., Rigo, O. D., Neto, C. M. & Mei, P. R. 2006. The effects of vacuum induction melting and electron beam melting techniques on the purity of NiTi shape memory alloys. *Materials Science and Engineering A* 438–440: 679–682. doi:10.1016/j.msea.2006.02.171

Pessard, E., Mognol, P., Hascoët, J. Y. & Gerometta, C. 2008. Complex cast parts with rapid tooling: Rapid manufacturing point of view. *International Journal of Advanced Manufacturing Technology* 39(9–10): 898–904. doi:10.1007/s00170-007-1281-8

Roach, D., Wong, J., Kuang, X., Hamel, C., Kovitz, J. & Qi, H. J. 2019. Developing intelligent structures and devices using novel smart materials and multi-material multi-method (M4) 3D printing. In *Structural Health Monitoring 2019: Enabling Intelligent Life-Cycle Health Management for Industry Internet of Things (IIoT)*, 965–972. doi:10.12783/shm2019/32209

Sagar, V. R., Lorin, S., Göhl, J., Quist, J., Cromvik, C., Mark, A., Jareteg, K., Edelvik, F., Wärmefjord, K. & Söderberg, R. 2020. Investigating the sensitivity of particle size distribution on part geometry in additive manufacturing. In *ASME International Mechanical Engineering Congress and Exposition (IMECE)*. doi:10.1115/IMECE2020-23816

Sagar, V. R., Lorin, S., Göhl, J., Quist, J., Jareteg, K., Cromvik, C., Mark, A., Edelvik, F., Wärmefjord, K. & Söderberg, R. 2022. A simulation study on the effect of particle size distribution on the printed geometry in selective laser melting. *Journal of Manufacturing Science and Engineering* 144(5). doi:10.1115/1.4052705

Speirs, M., Wang, X., Van Baelen, S., Ahadi, A., Dadbakhsh, S., Kruth, J.-P. & Van Humbeeck, J. 2016. On the transformation behavior of NiTi shape-memory alloy produced by SLM. *Shape Memory and Superelasticity* 2(4): 310–316. doi:10.1007/s40830-016-0083-y

Spierings, A. B., Herres, N. & Levy, G. 2011. Influence of the particle size distribution on surface quality and mechanical properties in AM steel parts. *Rapid Prototyping Journal* 17(3): 195–202. doi:10.1108/13552541111124770

Su, C., Li, X., Xu, C., Li, G., Cao, J., Li, X. & Huang, W. M. 2024. Optimization of selective laser melting (SLM) fabrication quality for Ti6Al4V alloy: Experimental and numerical study with introduction of remelting process. *The International Journal of Advanced Manufacturing Technology* 133(11–12): 5211–5231. doi:10.1007/s00170-024-14031-7

Swiercz, R. & Oniszczuk-Swiercz, D. 2024. Metal additive manufacturing—AFM postprocessing technology. *AIP Conference Proceedings* 3130(1). doi:10.1063/5.0204297

Tian, X., Li, D., Lian, Q., Wang, L., Lu, Z., Huang, K., Wang, F., Liang, Q., Zhang, H., Meng, Z., He, J., Sun, C., Liu, T., Huo, C., Wu, L. & Lu, B. 2024. Additive manufacturing of integrated micro/macro structures driven by diversified functions—30 years of development of additive manufacturing in Xi'an Jiaotong University. *Additive Manufacturing Frontiers* 3(2). doi:10.1016/j.amf.2024.200140

Valls, I. & Le Bourdiec, T. 2024. Cost-effective high-performance metal additive manufacturing: A technological and a sustainable opportunity for tooling of press hardening process. In *9th International Conference on Hot Sheet Metal Forming of High-Performance Steel (CHS2 2024)*, 66–73. doi:10.33313/512/A0403

Wang, H., Wu, X., Guo, X. Y., Tan, Z., Zhou, Z. & Shao, W. 2022. Characterization of pre-alloyed NiTi powders produced by electrode induction-melting inert gas atomization for additive manufacturing. *Journal of Mining and Metallurgy B: Metallurgy* 58(2): 219–228. doi:10.2298/JMMB211019006W

Wang, L., Wei, Q., He, W. & Shi, Y. 2012. Influence of powder characteristic and process parameters on SLM formability. *Journal of Huazhong University of Science and Technology (Natural Science Edition)* 40(6): 20–23.

Wang, L., Zhang, Y., Chia, H. Y. & Yan, W. 2022. Mechanism of keyhole pore formation in metal additive manufacturing. *npj Computational Materials* 8(1). doi:10.1038/s41524-022-00699-6

Wang, M., Yang, Y., Trofimov, V., Song, C., Zhou, H. & Wang, D. 2023. Effects of particle size on processability of AlSi10Mg alloy manufactured by selective laser melting. *Acta Metallurgica Sinica* 59(1): 147–156. doi:10.11900/0412.1961.2022.00442

Xiao, Z., Yang, Y., Xiao, R., Bai, Y., Song, C. & Wang, D. 2018. Evaluation of topology-optimized lattice structures manufactured via selective laser melting. *Materials and Design* 143: 27–37. doi:10.1016/j.matdes.2018.01.023

Yan, J., Cai, B., Ou, B., Meng, X., Xie, Y., Zhang, Y. & Fang, S. 2024. Effect of laser energy density on the phase transformation behavior and functional properties of NiTi shape memory alloy by selective laser melting. *Journal of Alloys and Compounds* 1005. doi:10.1016/j.jallcom.2024.176060

Yang, Y., Zhan, J. B., Li, B., Lin, J. X., Gao, J. J., Zhang, Z. Q., Ren, L., Castany, P. & Gloriant, T. 2019. Laser beam energy dependence of martensitic transformation in SLM fabricated NiTi shape memory alloy. *Materialia* 6. doi:10.1016/j.mtla.2019.100305

Yasa, E. & Kruth, J. 2011. Application of laser re-melting on selective laser melting parts. *Advances in Production Engineering & Management* 6: 259–270.

Yu, Z., Xin, R., Xu, Z., Zhu, Y., Zhang, X., Hao, S., Zhang, Z. & Liang, P. 2023. Investigation on the mechanical properties and shape memory effect of landing buffer structure based on NiTi alloy printing. *Chinese Journal of Mechanical Engineering* 36(1). doi:10.1186/s10033-023-00898-2

Zhan, J.-B., Lu, Y.-J. & Lin, J.-X. 2021. On the martensitic transformation temperatures and mechanical properties of NiTi alloy manufactured by selective laser melting: Effect of remelting. *Acta Metallurgica Sinica (English Letters)* 34(9): 1223–1233. doi:10.1007/s40195-021-01212-6

Zhang, C., Liao, Q., Zhang, X., Ma, F., Wu, M. & Xu, Q. 2023. Characterization of porosity in lack of fusion pores in selective laser melting using the wavefunction. *Materials Research Express* 10(1). doi:10.1088/2053-1591/acaf24

Zhang, L., Song, B., Fu, J. J., Wei, S. S., Yang, L., Yan, C. Z., Li, H., Gao, L. & Shi, Y. S. 2020. Topology-optimized lattice structures with simultaneously high stiffness and light weight fabricated by selective laser melting: Design, manufacturing and characterization. *Journal of Manufacturing Processes* 56: 1166–1177. doi:10.1016/j.jmapro.2020.06.005